Submitted: 15.12.2023.

Accepted: 11.01.2024.

Developing thermal insulation cement-based mortars with recycled aggregate in accordance with Net Zero principles

https://doi.org/10.2298/SOS231215002P

Marko Pavlović[1], Anja Terzić[2*], Marina Dojčinović[3], Dragan Radulović[4]

[1]Faculty of Mechanical Engineering, University of Belgrade – Innovation Center, Kraljice Marije 16, Belgrade, Serbia
[2]Institute for materials testing - IMS, Bulevar vojvode Mišića 43, 11000 Belgrade, Serbia
[3]Faculty of Technology and Metallurgy, University of Belgrade, Karnegijeva 4, 11000 Belgrade, Serbia
[4]Institute for Technology of Nuclear and Other Mineral Raw Materials, Franchet d'Esperey 86, 11000 Belgrade, Serbia
[*] corresponding author: anja.terzic@institutims.rs

Abstract The performance of thermo-insulation rendering mortars with alternations in ratios of powdered cordierite and talc was examined. The goal was to confirm that recycled kilnware cordierite can be reapplied in the mortar design without significant deterioration in performance in comparison with OPC mortar. Differential thermal analysis was employed for examining thermally induced reactions. The cavitation erosion, in testing sequences ranging from 30 to 120 minutes, was used to assess the compactness of the mortar structure. The physico-mechanical properties of experimental mortars were investigated. The morphologies of the mortar tablets upon cavitation were studied using a scanning electron microscope. It was established that cordierite and talc filler in amounts up to 20% enhance microstructural packing and mechanical strengths due to improved cementation and therefore contribute to cavitation erosion resistance. Higher amounts of talc cause structural degradation and mass loss during cavitation tests. Reducing manufacturing costs, energy consumption, and greenhouse gas emissions are the main objectives of the production of this waste-based construction composite, as the reuse of waste materials can help achieve a number of Sustainable Development Goals.

Key words: *alternative raw materials; sintering; differential thermal analysis; microstructure; cavitation testing.*

1. Introduction

The construction industry is constantly looking for innovative building materials with the ability to alleviate energy requirements, boost thermal insulation, and reduce CO_2 emissions. Due to the world's increased living standards and fast population expansion, the entire planet is currently facing serious energy crises and problems. One of the main industries known to contribute significantly to atmospheric carbon dioxide emissions, which in turn cause global warming, is the building industry [1, 2]. With resource scarcity and climate change as major concerns, the primary goal is to identify strategies for reducing CO_2 emissions in the construction industry through innovative applications of alternative raw

materials [3]. In the construction sector, the main strategy is to invest in materials that conform to ‘Net Zero’ and ‘Zero Waste’ principles [4, 5].

Thermal mortar is defined as a building material with thermal insulation capabilities. Its thermal conductivity should be lower than 0.2 W/mK at 10 °C, according to standard EN 998-1:2017 [6]. Thermal renders and thermal plasters are terms for thermal mortars used on the exterior or inside of structural elements [7–9]. Thermal mortars are frequently created according to mix design that include lightweight aggregates [10]. Mortars with aggregates made of expanded polystyrene have been the most commonly utilized and researched [11, 12]. Other research has looked into the thermal benefits of hemp and similar fiber materials [13], expanded clay [14], silica aerogel [15, 16], and perlite [17-19]. Some authors have compensated for the environmentally friendly aspects of reusing waste in construction materials by incorporating olive stones and plastic waste [20, 21] or waste rubber tires [22] into energy-efficient mortars. The challenge is to create normal-weight rendering mortars based on recycled raw materials that have mechanical and thermal properties similar to regular building mortars.

Cordierite is a magnesium iron aluminium cyclosilicate. Cordierite is almost exclusively composed of iron. Between Fe-rich sekaninaite and Mg-rich cordierite, there is a solid solution with the following series formula: $(Mg,Fe)_2Al_3(Si_5AlO_{18})$ to $(Fe,Mg)_2Al_3(Si_5AlO_{18})$ [23, 24]. Cordierite's superior resistance to thermal shock allows it to be employed at temperatures as high as 1200°C. It also has a low thermal conductivity and a low thermal expansion coefficient. Cordierite also possesses strong insulating qualities. It has a Mohs hardness of roughly 7, and it is highly resistant to creep [25]. Kiln “furniture” is commonly made with cordierite due to its remarkable resilience to thermal shock. Compared to standard kiln ware, cordierite ware weighs between 60% and 70% less. Such ceramic kilnware also allows faster heat transfer [26]. Electric heating elements and insulating equipment are frequently made from cordierite. For example, cordierite components are utilized in lighting technology, thermostats, and fuses [27]. Due to its ability for rapid heating and cooling sequences and its high resistance to thermal shock, cordierite is a preferred material for catalyst carriers, which are mostly used for purifying industrial and automobile exhaust [28]. Cordierite, which typically takes the shape of ceramic foam or honeycombs, is ideal for filtering molten metal. It also shows the ability to decrease the level of contaminants and purify liquid metal [29].

When considering all relevant factors, such as the appropriate use of the secondary raw material, the end product's economic feasibility, and its environmental impact, the application of recycled materials in the building industry can be challenging. Thermal insulation rendering mortars have been designed with a wide range of waste raw materials, as was previously brought up [13, 20–22]. One topic that has yet to be properly investigated is the reapplication of waste cordierite from kilnware as coarse aggregate in the mortar design. Typically, three-fourths of the volume of the mortar is composed of natural aggregates, both fine and coarse. Often, it may not be cost-effective to prepare artificial aggregates for thermal insulation mortars. Therefore, a smart way to solve this issue is to look for substitute materials for aggregates, i.e., materials that are typically derived from industrial operations and considered waste. Cordierite kilnware, which is usually disposed of in factory landfills, can be used in place of coarse aggregate. In combination with fillers, this industrial waste can provide the basis for the design of novel thermal insulation materials. In this study, ordinary Portland cement was mixed with coarse cordierite aggregate and pulverized cordierite, while talc was employed as a mineral additive. Because talc powder is lightweight and has moisture-controlling qualities, it is often used in thermal insulation applications. It has the capacity to decrease heat transfer, enhance tensile strength, and lessen thermal energy conduction. The refractory mortar's adhesion, impermeability, and volume stability are all

improved by the addition of talc powder. This enhances the resistance to rapid temperature changes, thermal fatigue, and water absorption [30–33].

The performance of rendering mortars with varying powdered cordierite and talc ratios (9:1, 4:1, and 2:1) was examined in this research. Differential thermal analysis was employed for examining thermally induced reactions. The cavitation erosion test was used to assess the compactness of the mortar structure. The morphology of mortar samples was studied using a scanning electron microscope. Reducing manufacturing costs, energy consumption, and greenhouse gas emissions are the main objectives of production of this innovative waste-based construction composite. The use of waste materials solves the issue of natural resource depletion and frees up landfill space for other uses. Also, reusing waste materials can help achieve a number of Sustainable Development Goals [34], such as tackling climate change (SDG 13), promoting responsible consumption and production (SDG 12), and sustaining life on land (SDG 15).

2. Experimental – materials and methods

2.1. Raw materials and thermal insulation composites

Four cement mortars were prepared for the experiment. Ordinary Portland cement (OPC) was used as the bonding agent in the design of all four mortars. The CEM I 42.5R from Lafarge was employed. The cement's specific surface area was 2250 cm^2/g, with 98% of the particles being smaller than 50 µm in diameter and an average grain diameter of 15 µm. The IM-CQ sample, which contained OPC and quartz aggregate, was used as a reference sample. The high-purity quartz sand (SiO_2 = 98.8%) showed the following properties: loose bulk density 1670 kg/m^3, compacted bulk density 1760 kg/m^3, and Mohs hardness 7. Recycled cordierite aggregate was obtained by crushing used kilnware, i.e., spiral cordierite ceramic heaters [35] by means of laboratory jaw crushers. Compacted bulk density of the cordierite samples was 2000 kg/m^3. Mohs hardness of cordierite is 7 – 7.5. The recycled aggregate was then sieved to obtain grain sizes of 2-4 mm, 1-2 mm, 0.5-1 mm, and 0.63-0.5 mm. The grain-size distribution of aggregate was determined by Tyler's series of sieves (Fig. 1.).

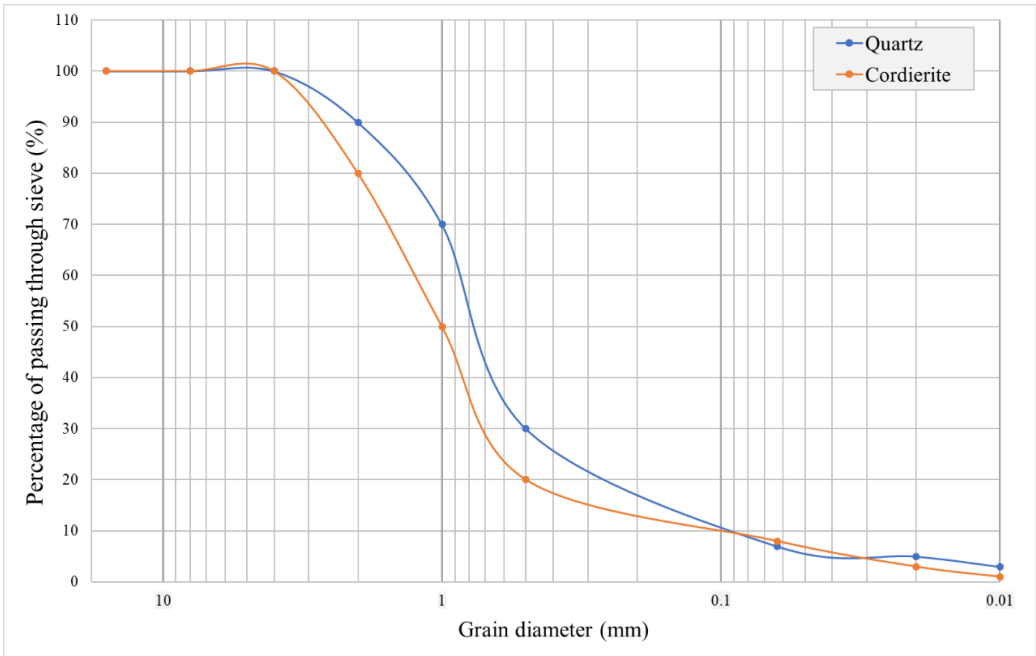

Fig. 1. Grain-size distribution of aggregate for thermal insulation composites.

Recycled cordierite powder and talc were used as fillers in thermal insulation composites (i.e., mortar samples IM-CrT10, IM-CrT20, and IM-CrT30). Because of its lightweight nature and ability to control moisture, talc powder is used as additive to improve thermal insulation properties. Talc also improves adhesion, impermeability, and volume stability in high-temperature mortars. Recycled cordierite and talc samples were pulverized by an ultra-centrifugal mill (Retsch ZM-1). The obtained BET-specific surface areas for cordierite and talc were 2995 cm^2/g and 3100 cm^2/g, respectively. Mean diameters for pulverized cordierite and talc samples were 11.5 μm and 10.2 μm, respectively. Filler was used in the amount of 20% of the cement mass. Talc was used in quantities of 10, 20, and 30% of the filler mass.

The chemical compositions of OPC, recycled cordierite, and talc were determined by the atomic emission spectroscopy technique on a Perkin Elmer PinAAcle 900 instrument. The results are presented in Table I.

Table I Chemical analysis of component materials for thermal insulation composites.

Oxide (%)	SiO_2	Al_2O_3	Fe_2O_3	CaO	MgO	K_2O	Na_2O	TiO_2	SO_3	LoI
OPC	21.93	5.42	3.04	62.95	2.52	0.92	0.1	0.1	2.13	0.89
Cordierite	51.18	30.14	1.17	3.19	13.21	0.01	-	-	-	1.08
Talc	60.79	4.05	0.7	1.05	31.3	0.01	-	-	-	2.1

* LoI = loss on ignition at 1000 °C

The mix design of the experimental mortars is given in Table II.

Table II Mix-design of the experimental mortar samples.

Sample	OPC (%)	Quartz agg. (%)	Cordierite agg. (%)	Cordierite filler (%)	Talc filler (%)
IM-CQ	40	60	-	-	-
IM-CrT10	32	-	60	7.2	0.8
IM-CrT20	32	-	60	6.4	1.6
IM-CrT30	32	-	60	5.6	2.4

2.2. Preparation of the thermal insulation composites and physico-mechanical testing

The procedure given in [36] was used to prepare mortar samples. Cement, aggregate, and filler were initially dry-homogenized in a laboratory mixer. Later during the mixing procedure, water was added. Water-to-cement ratio was kept 0.5 for all experimental mortar mixes. Fresh mortar was placed in steel molds (40×40×160 mm) and stored for one day in a climate chamber (95±5% relative humidity and 20°C (+3°C/-2°C) temperature. After being removed from the molds, the samples were kept in the climate room for 7 days under the same conditions. The samples were then cured for 21 days at 65±5% relative humidity.

Additionally, hardened mortar samples were fired in a Carbolite laboratory chamber furnace. The temperature range was 20–1000°C. The following regime was employed: constant heating rate of 10°C/min up to 800°C; constant heating rate of 5°C/min from 800°C to 1000°C; and 1 hour delay at maximal temperature.

The cavitation samples were cylinders with a diameter of 10 mm and a height of 10 mm. These samples underwent previously described thermal treatment.

A slump test with a flow table was used to determine the rheology of the fresh mortar [37]. Standard methods were used to calculate the bulk density of fresh mortar and the dry bulk density of hardened mortar [38, 39], the capillary water absorption coefficient [40], and the compressive and flexural strengths [41, 42]. The compressive strengths of sintered mortar samples were also determined.

2.3. Cavitation erosion resistance testing

Standard test method for cavitation erosion according to ASTM G32-16 [43] was employed on the experimentally prepared mortar samples IM-CQ, IM-CrT10, IM-CrT20, and

IM-CrT30. Since the tested material was brittle, the ultrasonic vibratory cavitation method with a stationary sample was chosen [44, 45]. The sample holder was fixed to the water bath's bottom. The mechanical vibratory concentrator was immersed in a water bath. The water temperature was kept constant at 25 ±1 °C. A 0.5 mm gap separated the sample from the front surface of the vibratory concentrator. Mechanical vibrations were utilized at a frequency of 20 kHz and an amplitude of 50 μm. A strong cavitation zone was formed underneath the front surface of the concentrator and the stationary-tested sample. The water from the water bath was cooling the sample to keep it at a consistent temperature. A continuous water flow generated a pressure field, which stimulated the implosion of cavitation bubbles on the surface of the mortar sample. The cavitation periods employed were 0, 30, 60, 90, and 120 min. Upon each testing the samples were dried and the mass loss was measured with an analytic accuracy of ±0.1 mg. The test output represents an average of minimum three testing per sample.

2.4. Instrumental methods

Differential thermal analysis was conducted on the pulverized hardened mortar samples (loose powder) using a SETSYS TG/DTA/DSC apparatus (SETARAM Instrumentation). Samples were placed in an alumina pan and heated from 20 °C up to 1000 °C. The heating rate was 10 °C/min. The analysis was conducted in the static airflow.

Scanning electron microscopy (SEM) analysis was conducted on the mortar samples (pelettes) upon cavitation. The testing samples were coated with carbon in 20 nm layer (density 2.25 g/cm^3). The textural analysis was conducted on a SEM instrument, the JEOL JSM-6610LV. The magnification of the device is 5 to 300,000 times. The electron source is W wire, LaB 6. The voltage is 0.3–30 kV. The instrument works with a vacuum system: a rotary pump and turbomolecular pump, an ion pump (used for LaB6), and a rotary pump for working in low vacuum (10–270 Pa). Detectors are: SE, BSE and CL.

3. Results and discussion

The thermally induced behaviour of experimental mortars IM-CQ, IM-CrT10, IM-CrT20, and IM-CrT30 was assessed by means of differential thermal analysis (Fig. 2). Samples were recorded in a thermal interval from 20°C to 1000°C. Various effects were observed during recording. The main peaks of the endothermic or exothermic processes are listed in Table III.

The DTA early effects (Fig. 2) are set at around 100°C. Aside from the initial water loss that occurs below 100°C, the earliest impacts are mainly related to the dehydration of AH_3H_2O gel, which takes place around 120°C. Ettringite and colloidal C-S-H gel form at temperatures ranging from 100°C to 150°C [46].

In the standard IM-CQ mortar, the first endothermic effect (peak 1) takes place at 99.2°C. It is followed by a very small and barely detectable effect (peak 2) at 149.5°C. For the sample IM-CrT10, peak 1 is set at a lower temperature (Table III). This indicates a faster reaction, i.e., a faster release of the free water from the treated mortar sample. The samples IM-CrT20 and IM-CrT30 showed similar behavior, with their initial endothermic peaks being set at 70.2°C and 65.2°C, respectively. This indicates that the loss of water and the entire hydration reaction in composite mortars (mortars with the addition of cordierite and talc) take place at lower temperatures than in OPC-based mortar. Also, the peak 2 in each of the composite mortars is significantly more pronounced than that of the IM-CQ sample. This occurrence indicates the higher intensity of the energy released during the initial reactions of early hydration.

The addition of talc filler brought about certain changes in the behavior of the experimental thermal insulation mortars. Talc possesses both adsorption water and hydroxyl

groups in its structure, which constitute the space lattice elements. Water is generally lost throughout the three phases of dehydration (115°–200°C, 350°–500°C, and 600°–1050°C). As a result, the reactions are followed by three endothermic peaks observed on the DTA curve [47]. Thereby, the occurrence of exothermic peak 7 in all composite mortars (IM-CrT10, IM-CrT20, and IM-CrT30) can be related to the loss of water from the talc structural lattice. Corundum exhibits no phase changes at low temperatures; however, it is possible that a share of amorphous alumino-silicates from its composition participate as additional pozzolana in early reactions (formation of ettringite and colloidal C-S-H gel) and influence the increase in hydration rate. The early reactions are also less energy-demanding in comparison with the reactions that took place in standard OPC mortar (IM-CQ).

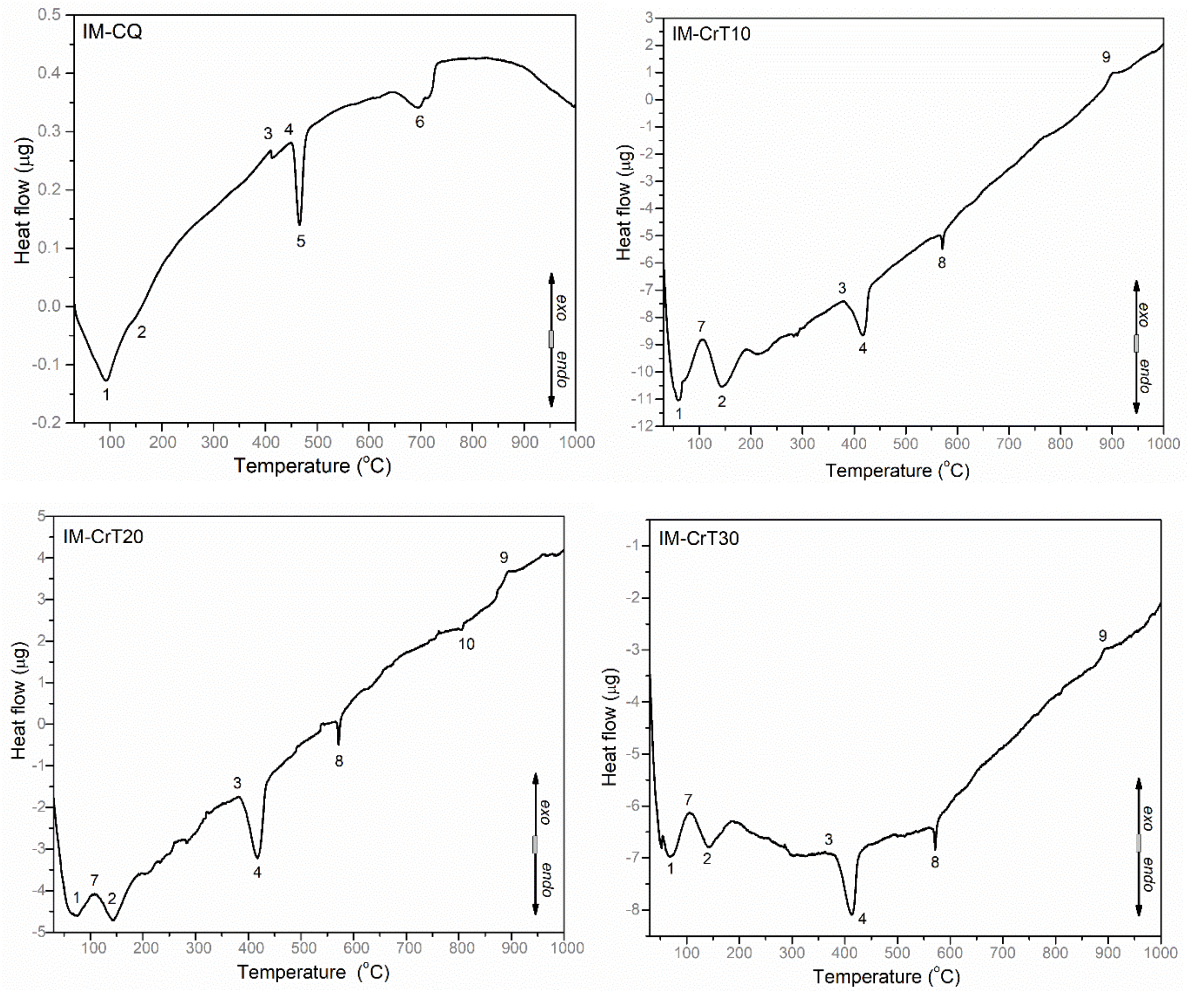

Fig. 2. DTA curves of mortar samples IM-CQ, IM-CrT10, IM-CrT20, and IM-CrT30.

Table III Positions of peaks in DTA curves (Fig.2)

Peak No.	1	2	3	4	5	6	7	8	9	10
IM-CQ	99.2°C	149.5°C	408.9°C	450.5°C	487.9°C	691.2°C	-	-	-	-
IM-CrT10	68.7°C	150.1°C	392.5°C	420.9°C	-	-	103.9°C	590.2°C	895.4°C	-
IM-CrT20	70.2°C	149.3°C	395.1°C	425.3°C	-	-	108.7°C	593.4°C	901.5°C	805.2°C
IM-CrT30	65.2°C	148.1°C	385.6°C	410.5°C	-	-	105.4°C	580.1°C	891.7°C	-

The next stage of thermally induced reactions occurs in the 400–500°C range. Dehydration of calcium aluminate and alumina hydrates takes place around 500°C, depending on mineral additions, which is commonly coincident with an endothermic effect

on a DTA curve [48, 49]. This can be correlated with peaks 3, 4, and 5. The endothermic maximum for IM-CQ is identified at 487.9°C (peak 5). This peak is absent from the rest of the samples. Peaks 3 and 4 of the composite mortars are all shifted towards lower temperatures in comparison to those of IM-CQ, indicating that hydration processes in the IM-CrT10, IM-CrT20, and IM-CrT30 samples are more rapid.

A small exothermic hump rising above 500°C can be seen in the DTA diagram of the IM-CQ sample. The effects at this temperature are usually associated with the α- to β-quartz polymorphic transition (573 °C, precisely, in a pure quartz sample) [50]. All investigated mortar samples have significant amounts of SiO2 in their composition. The samples IM-CrT10, IM-CrT20, and IM-CrT30, besides exothermic hump, exhibit a needle-like peak at approximately 590°C (peak 8), which can be correlated to the supplementary amount of crystalline quartz from pulverized cordierite kilnware addition. The peak 6 appearing in the sample IM-CQ probably corresponds to the decomposition of $Ca(OH)_2$, which started above 450°C. This peak is absent from the IM-CrT10, IM-CrT20, and IM-CrT30 samples due to the lower amount of calcium in their compositions. Calcination of calcite ($CaCO_3$) is usually completed at 890°C [51, 52]. IM-CQ mortar exhibits an exothermic hump at approximately 800°C without a well-defined peak. The DTA curves of the IM-CrT10, IM-CrT20, and IM-CrT30 samples display a constant rise, with several small peaks appearing on the recorded curve. Peak 10 visible on the DTA curve of the IM-CrT20 sample can be correlated with talc decomposing into magnesium oxide and silica due to the liberation of its structural-bonded water [53, 54]. Exothermic peaks (peak 9) appearing above 880°C in IM-CrT10, IM-CrT20, and IM-CrT30 samples can be described as the initiation of a solid-state reaction that leads to the cordierite phase transformation [55]. The sample IM-CrT20 exhibited the most rapid thermally induced reactions and thereby the quickest hydration route, probably due to the amorphous alumino-silicate (i.e., additional pozzolana) from cordierite filler [56].

A cavitation test was conducted on the IM-CQ, IM-CrT10, IM-CrT20, and IM-CrT30 samples. Figure 3 depicts the surfaces of IM-CrT20 (1), IM-CrT30 (2), IM-CQ (3), and IM-CQ (4) after cavitation erosion with water for 0, 30, 60, 90, and 120 minutes.

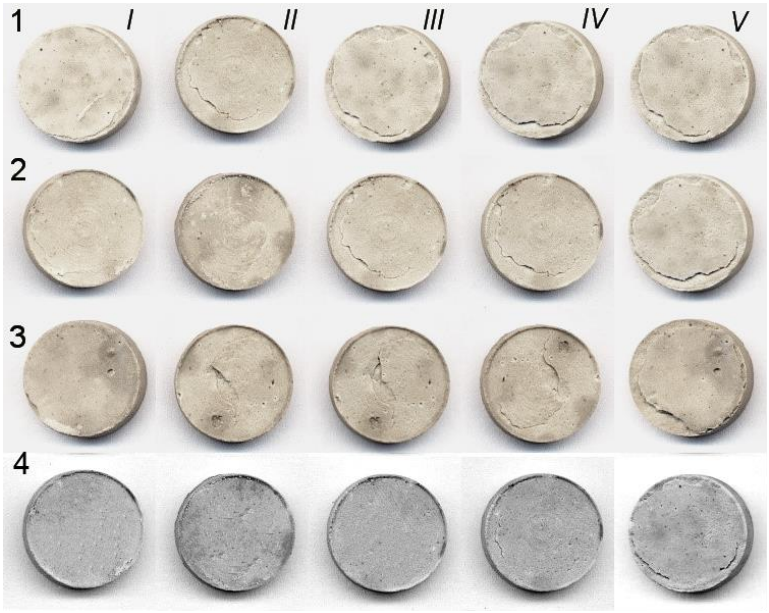

Fig 3. Surface of the samples IM-CrT10 (1), IM-CrT20 (2), IM-CrT30 (3), and IM-CQ (4) upon 0 (I), 30 (II), 60 (III), 90 (IV), and 120 (V) minutes long cavitation erosion.

As it can be seen, all tested samples predominantly maintained their structural integrity. The mechanical strengths of the IM-CQ, IM-CrT10, IM-CrT20, and IM-CrT30

samples were high enough to sustain the water pressure, and therefore no breaking of the samples was recorded during the projected testing intervals. The visual examination of each sample exhibited in Fig. 2 leads to the conclusion that certain visible major cracks are present.

After 30 minutes of erosion, a massive superficial crack emerged on the sample IM-CrT10 (1). During the subsequent 30 minutes of erosion (i.e. testing II = 60 minutes), the fracture did not change significantly in shape or depth. After 90 minutes, the sample 2 developed superficial delamination, first in the top left corner. After 120 minutes, the delamination had spread to the whole upper portion of the tablet. The fracture begins to emerge around it, but it does not appear to become significantly deeper.

The initial 30 minutes of cavitation erosion produced no damage to the surface of the sample IM-CrT20 (2). After 60 minutes of exposure, a thin, superficial fracture emerged. During the subsequent erosion interval (90 minutes), the crack remained unchanged. After 120 minutes of erosion, delamination surrounding the fracture appeared.

After 30 minutes of erosion sequences, a notable superficial delamination appeared in the middle of the IM-CrT30 (3) tablet. This delamination retains its shape and size during the 60-minute erosion sequence. After 90 minutes, a crack started opening on the sample's surface. The water erosion treatment smoothed the surface after 120 minutes. A deep crack appeared near the edge of the tablet while the corners started to chip off, indicating that the sample will shatter with more prolonged treatments.

The sample IM-CQ (4) showed different behaviour due to its different mix design. The sample remained unchanged for up to 90 minutes of cavitation erosion. During this sequence, the first cracks started to appear. 120-minute cavitation sequence led to more significant damage, which was visually similar to that of samples IM-CrT10 and IM-CrT20 after equally long treatments.

The cavitation erosion of the mortar samples IM-CQ, IM-CrT10, IM-CrT20, and IM-CrT30 was expressed numerically as mass loss recorded after 30, 60, 60, and 120 minutes of testing. Table IV shows the numerical results for mass loss and cavitation velocities. For each series of tests, three samples were used, and the results show the mean value of these measures for each test interval. Figure 4 depicts a histogram of mass loss per testing sample as a function of cavitation duration. The cavitation velocity is determined using the ASTM G32-16 standard as the total mass loss divided by the testing period. Figure 5 depicts the cavitation velocities for each testing mortar type.

Table IV. Cavitation erosion measurements performed on the mortar samples.

Sample	IM-CQ	IM-CrT10	IM-CrT20	IM-CrT30
Initial mass (mg)	2270	2280	2275	2260
Time (min)	Mass loss (mg) / Cavitation velocity (mg/min)			
0	0 / 0	0 / 0	0 / 0	0 / 0
30	11.35 / 0.36	12.87 / 0.34	12.34 / 0.35	15.12 / 0.41
60	24.51 / 0.40	25.79 / 0.38	24.87/ 0.39	28.61 / 0.45
90	36.54 / 0.39	38.53 / 0.37	37.68 / 0.38	40.98 / 0.48
120	48.20 / 0.38	49.25 / 0.36	48.71 / 0.37	52.45 / 0.51
Avg. velocity (mg/min)	0.3825	0.3625	0.3725	0.4625

As expected, the mass loss per sample increased as cavitation erosion duration increased. If sample IM-CQ is a representative standard mortar sample, it can be concluded that mortars designed with recycled raw materials showed a very small deviation in behavior in comparison to 'standard'. Namely, 'recycled' mortars IM-CrT10 and IM-CrT20 showed 13% and 12%, respectively, higher mass loss than IM-CQ. The mass loss of the IM-CrT30 sample in compression with that of IM-CQ was notably higher, amounting to 33%. Differences for 60- and 90-minute treatment were similar: 5%, 1.4%, 16%, and 5%, 3%, and

12% for samples IM-CrT10, IM-CrT20, and IM-CrT30, respectively. Final cavitation erosion treatment produced differences in mass loss as follows: 2%, 1%, and 8% in IM-CrT10, IM-CrT20, and IM-CrT30, respectively. The sample IM-CrT20 showed minimal mass loss in comparison with standard cement mortar.

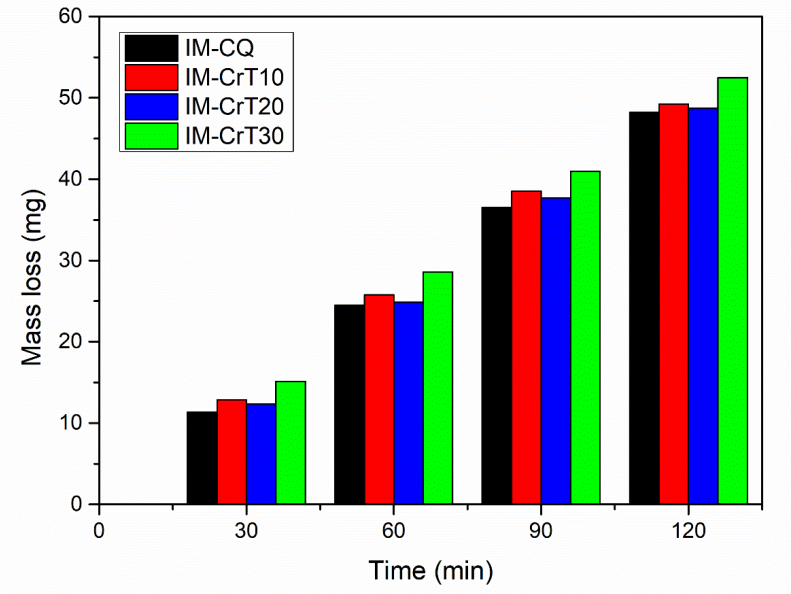

Fig. 4. Mass loss per testing sample as a function of cavitation duration.

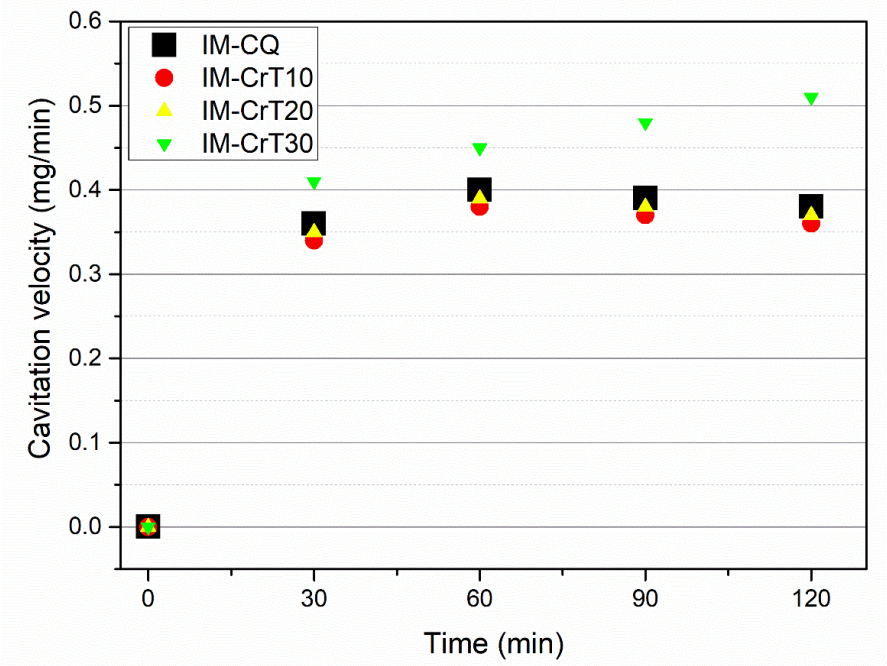

Fig. 5. Comparison of cavitation velocities for each tested mortar type.

As it can be seen in Fig. 5, cavitation velocity (i.e., mass loss during the indicated time period) was highest for the IM-CrT30 sample. This means that a 30% addition of talc filler made the structure of the materials more loose and therefore more susceptible to cavitation erosion. For the rest of the samples, including standard OPC mortar (IM-CQ), cavitation velocities ranged in a tight interval from 0.35 mg/min to 0.41 mg/min. This means that the application of recycled cordierite filler, cordierite aggregate, and talc filler in amounts of 10% and 20% did not significantly influence the deterioration of the mortar structure. Thereby, cordierite filler and talc filler in amounts up to 20% improve microstructural

packing and probably mechanical strengths due to more effective cementation, and thereby contribute to cavitation erosion resistance. Application of talc in higher percentages (e.g., 30 %) leads to notable structural degradation during cavitation testing and significant mass loss.

Histograms representing tested physico-mechanical properties (workability, bulk density of fresh mortar, bulk density of hardened mortar, and water absorption coefficient) of mortar samples (IM-CQ, IM-CrT10, IM-CrT20, and IM-CrT30) are given in Figure 6.

In comparison to standard cement mortar (IM-CQ), the workability of fresh mortar samples decreased with the amount of added talc filler. The workability of the IM-CQ sample was 190 mm. The workability decreased by 3% with the addition of 10% of talc filler (IM-CrT10). The values of workability for samples IM-CrT20 and IM-CrT30 were 4% and 6% smaller than those of IM-CQ. The filler made the consistency of the fresh mortar stiffer and more water-demanding. Bulk density, measured both in fresh and hardened states, also showed a decreasing trend. IM-CrT10, IM-CrT20, and IM-CrT30 samples had somewhat lower bulk density values than IM-CQ, which were 2300 kg/m^3 and 2240 kg/m^3 in fresh and hardened states, respectively. The values decreased by 2%, 3%, and 5% for the IM-CrT10, IM-CrT20, and IM-CrT30 samples, respectively, in their fresh condition. Hardened samples showed similar interrelationships: 3%, 4%, and 7%. The values of the water absorption coefficient are decreasing with the increasing content of filler. The addition of filler aided in better 'packing' of the microstructure, leaving fewer voids and pores behind and lowering the examined material's water absorption capability. Besides that, talc is lightweight and has moisture-controlling qualities. It has the capacity to improve mortar's impermeability, volume stability, and resistance to water absorption. [30–33].

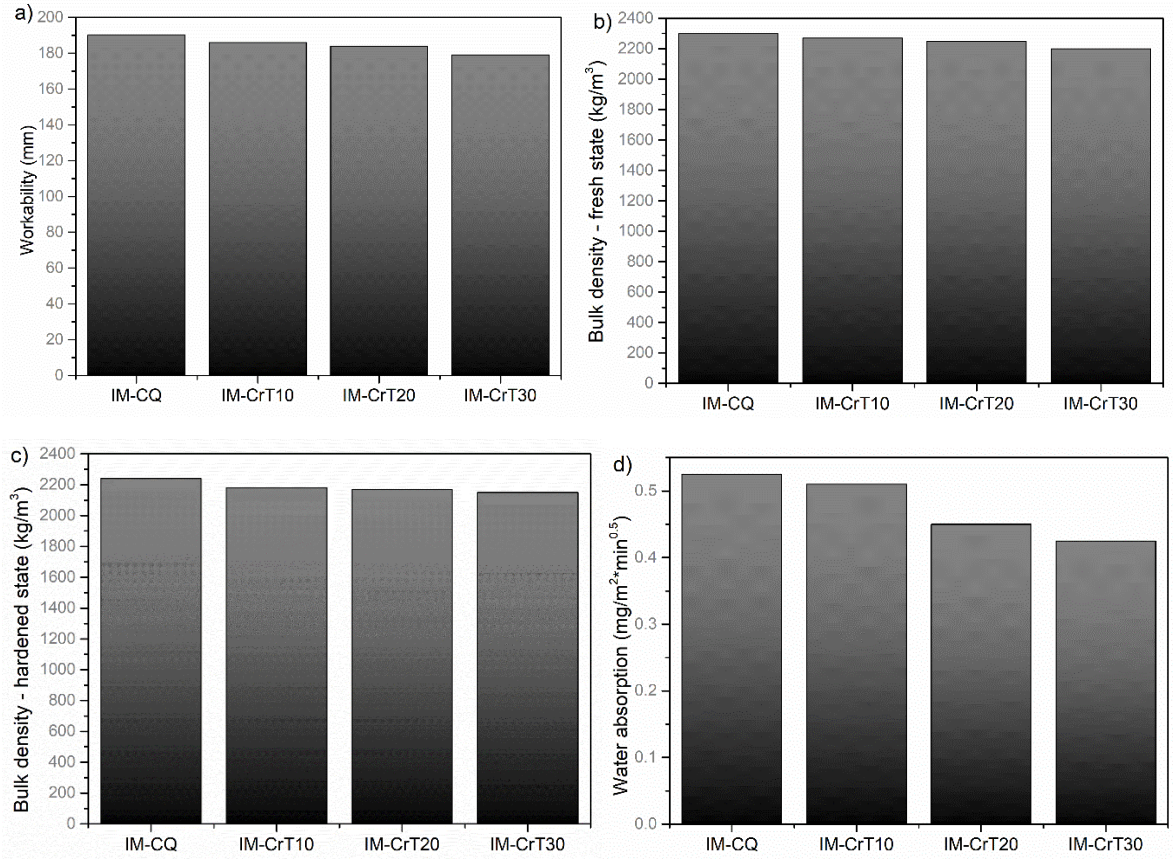

Fig. 6. Physico-mechanical properties of mortar samples: a) workability, b) bulk density of fresh mortar, c) bulk density of hardened mortar, d) water absorption coefficient.

A histogram representing the mechanical strengths of tested mortars is provided in Fig. 7. CS is compressive strength measured after 2, 7, and 28 days of hardening; FS is flexural strength measured after 2, 7, and 28 days of hardening; and CS-1000 is compressive strength measured after thermal treatment at 1000°C.

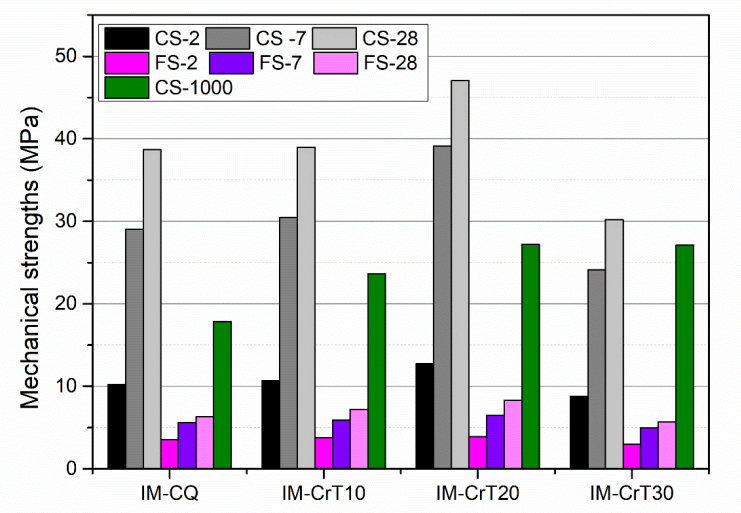

Fig. 7. Mechanical strengths of mortar samples.

As shown in Fig. 9, differences in compressive strengths were not significantly pronounced during the early stages of mortar hardening. After two days of hardening, the compressive strength of the IM-CrT10 sample was 4% lower than adequate mechanical strength of IM-CQ mortar. There is a 15% difference in CS-2 between IM-CrT30 and IM-CQ. The initial compressive strength of IM-CrT30 is the lowest of all measured values, counting up to 8.75 MPa. The CS-2 value for IM-CrT20 is the highest (12.75 MPa) and 24% higher than the CS-2 strength of OPC-based mortar. Thereby, the combination of cordierite filler and talc filler in the amount of 20% influenced the increase in early compressive strengths. The interrelationships between initial flexural strengths are slightly different. Namely, the FS-2 flexural strengths of IM-CrT10 and IM-CrT20 were 7% and 10% higher than those of IM-CQ mortar. A higher increase in initial strengths can be explained by the pozzolanic effect of cordierite filler and its influence on the early hydration mechanism.

The IM-CrT20 sample exhibited the highest final compressive strength (CS-28 = 47.05 MPa), indicating that the talc filler contributed the most in its quantity of 20%. Thereby, quantities over 20% of talc have no beneficial effect on mechanical strengths. Namely, the final compressive strength (CS-28) for the IM-CrT30 sample was 22% lower than the CS-28 of standard OPC mortar. Similarly, IM-CrT20 showed the highest value of FS-28 (8.3 MPa). The difference between the values of the final flexural strengths of IM-CQ and IM-CrT30 was 10%.

Cordierite and talc filler improved the compressive strengths of mortars fired at 1000°C. The values of CS-1000 were 32%, 52%, and 51% higher for IM-CrT10, IM-CrT20, and IM-CrT30 mortars, respectively, in comparison to CS-1000 of the IM-CQ sample. This occurrence can be explained by the advanced refractory properties and behaviour of both cordierite and talc.

The morphology and textural characteristics of the mortar samples prior to cavitation erosion and upon cavitation erosion were investigated via SEM microstructural analysis. The SEM microphotographs are given in Fig. 8.

SEM microphotographs revealed that the structural integrity of the IM-CrT10, IM-CrT20, and IM-CrT30 samples was mostly preserved. There are no huge voids, microcracks, or extremely disrupted superficial parts of the examined samples. The microstructure of the

initial samples (Fig. 8 a, d, and g) looks similar. Cordierite gains (originating from aggregate) are immersed in cement matrix combined with filler particles. The IM-CrT20 sample has a denser structure than the rest of the samples, which can be endorsed by the highest value of mechanical strength after firing at 1000°C (Fig. 7). The structure of IM-CrT30 seems to be more vitrified. Cavitation erosion lasting 60 minutes (Fig. 8 b, e, and h) caused the formation of small pits due to the loss of superficially positioned grains. Namely, the water stream and air bubbles created around mortar tablets induced a decrease in the bond strength of superficial cordierite grains and cement matrix, which led to grains' falling out and eventually to a certain mass loss of a sample. Pits are clearly visible on the middle-left side of Fig. 8b (sample IM-CrT10). Sample IM-CrT20 (Fig. 8e) exhibited comparatively smaller pits because the water stream managed to remove only small superficial particles due to the more vitreous nature of the sample. In the microphotograph of the sample IM-CrT30, the appearance of certain delamination can be assumed, which is in accordance with the highest mass loss for this sample (values provided in Fig. 4). 120 minutes of cavitation erosion led to further superficial material loss in all of the presented samples (Fig. 8 c, f, and i), but no critical structural damage was identified.

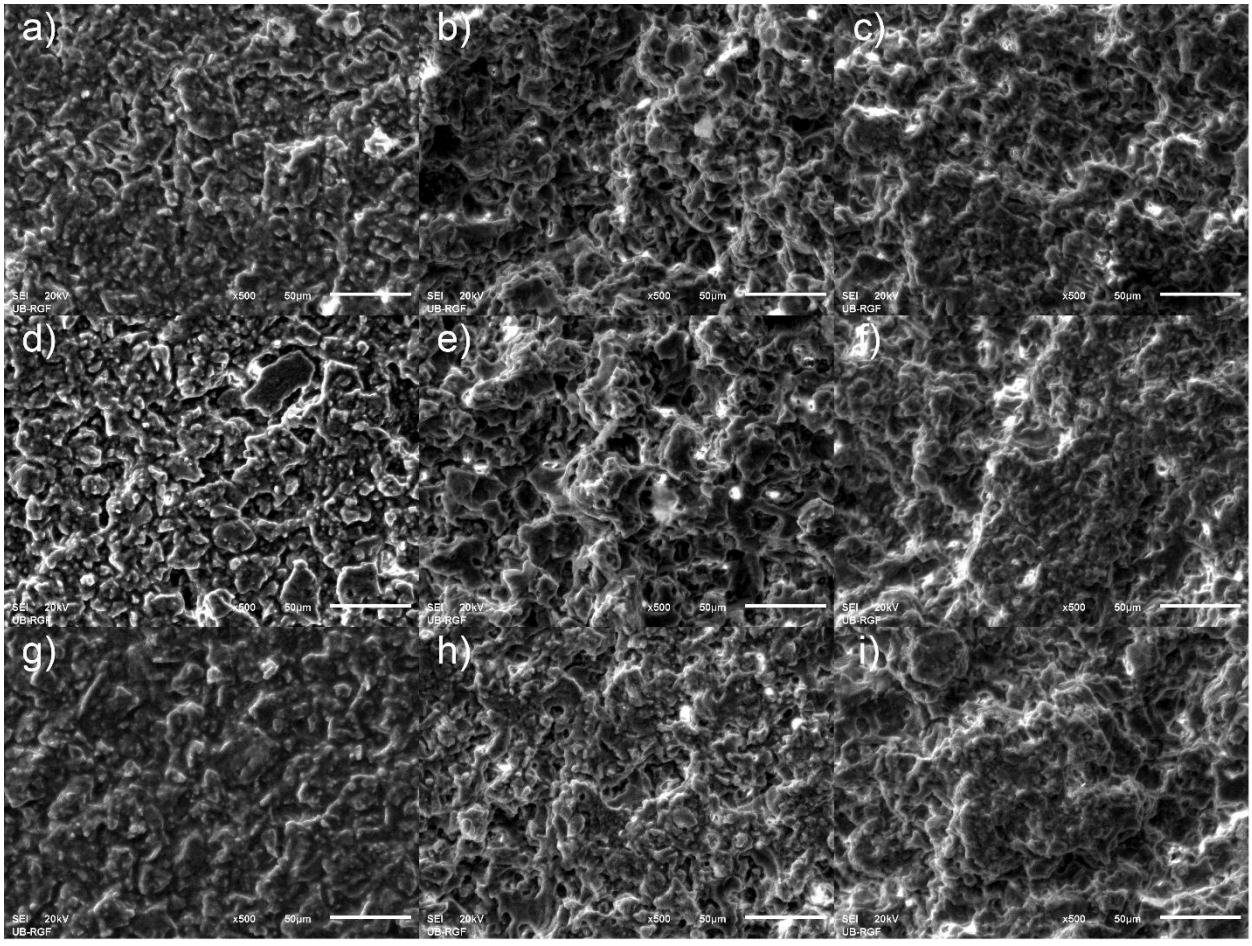

Fig. 8. SEM microphotographs of: IM-CrT10 (a) initial sample; b) 60 min cavitation; c) 120 min cavitation), IM-CrT20 (d) initial sample; e) 60 min cavitation; f) 120 min cavitation), and IM-CrT30 (g) initial sample; h) 60 min cavitation; i) 120 min cavitation) mortars.

4. Conclusions

This study confirmed that recycled cordierite from kilnware can be reapplied in the mortar design without significant deterioration of the properties in comparison with standard OPC-based mortar. The main conclusions are summed up below:

- Differential thermal analysis highlighted that the sample which included 20% of talc in its mix design (IM-CrT20), exhibited the most rapid thermally induced reactions and thereby the quickest hydration route due to the amorphous alumino-silicate (i.e., additional pozzolana) from cordierite filler. All recycled mortars (IM-CrT10, IM-CrT20, and IM-CrT30) were characterized by quicker hydration mechanisms than standard OPC-based mortar (IM-CQ).
- All experimental samples predominantly maintained their structural integrity during cavitation erosion testing in comparison to the IM-CQ sample. The mechanical strengths of the IM-CrT10, IM-CrT20, and IM-CrT30 mortars were high enough to sustain the water pressure, and therefore no breaking of the samples was recorded during the projected testing intervals (up to 120 min).
- The sample IM-CrT20 showed minimal mass loss (only 1%) in comparison with standard cement mortar after the final cavitation sequence.
- The measured cavitation velocities ranged from 0.35 mg/min to 0.41 mg/min. As a result, the use of recycled cordierite filler, cordierite aggregate, and talc filler in amounts of 10% and 20% had no effect on the deterioration of the mortar structure. Cordierite and talc fillers in amounts up to 20% enhance microstructural packing and mechanical strengths due to improved cementation and therefore contribute to cavitation erosion resistance. Higher amounts of talc (e.g., 30%) cause more significant structural degradation and mass loss during cavitation tests.
- The study demonstrated that ceramic kilnware waste can be repurposed and reused. In terms of circular economy principles, this waste raw material offers a high re-utilization potential, so it is critical to thoroughly investigate it and subsequently optimize manufacturing process of commercial products.

Acknowledgments: The authors gratefully appreciate support from the projects financially supported by the Ministry of Science, Technological Development and Innovation of the Republic of Serbia (Contract No.: 451-03-47/2023-01/200012, 451-03-47/2023-01/200213, and 451-03-47/2023-01/200135) and 101111694 -GREENCO - ERASMUS-EDU-2022-PI-ALL-INNO. The authors would like to express mutual gratitude to laboratories and colleagues from Institute of Technical Sciences SANU, Belgrade for recording DTA diagrams.

5. References

1. Global Status Report for Buildings and Construction: https://www.unep.org/resources/publication/2022-global-status-report-buildings-and-construction
2. S. Dora, K.M. Mini, J. Energy Storage 72 (2023)108550.
3. A. Liebringshausen, P. Eversmann, A. Göbert, J. Build. Engin. 80 (2023) 107696.
4. A. P. Galvín, S. Sabrina, B. Auxi, A. Peña, A. López-Uceda, J. Environ. Manag. 344 (2023) 118409.
5. E. Marsh, J. Orr, T.Ibell, Energy and Buildings 251 (2021) 111340.
6. European Committee for Standardization, EN 998-1:2017 - 'Specification for mortar for masonry - Part 1: Rendering and plastering mortar. British Standards Institution (2017).
7. A. Henry, J. Stewart, English Heritage (2011) https://doi.org/10.1080/13556207.2014.858292
8. A. Ranesi, R. Veiga, P. Faria, Constr. Build. Mater. 304 (2021), 124595.
9. A. Terzić, M. Dojčinović, Lj. Miličić, J. Stojanović, Z. Radojević, Sci. Sinter. 53:04 (2021) 445.
10. X. Hu, Materials Today: Proceedings 22:4 (2020) 2539.
11. J. Maia, N.M.M. Ramos, R. Veiga, Build. Environ. (2018) https://doi.org/10.1016/j. buildenv.2018.08.055.

12. M.G. Gomes, I. Flores-Colen, H. Melo, A. Soares, Constr. Build. Mater. 198 (2019) 786.
13. B. Mazhoud, F. Collet, S. Pretot, J. Chamoin, Build. Environ. 96 (2016) 206.
14. F. Yu, Y. Chen, Y. Fang, P. Xu, B. Xu, Q. Liu, J. Build. Engin.74 (2023)106930.
15. J. Maia, et al., Energy Build. 243 (2021) https://doi.org/10.1016/j.enbuild.2021.111001.
16. Ş. O. Kalkan, L. Gündüz, Constr. Build. Mater. 409 (2023) 134066.
17. A. Terzić, J. Stojanović, Lj. Andrić, Lj. Miličić, Z. Radojević, Sci. Sint. 52:2 (2020) 149.
18. M.L. Torres, P.A. García-Ruiz, Cem. Concr. Compos. 31(2009) 2.
19. G. Jia, J. Guo, Z. Li, Constr. Build. Mater. 394 (2023) 132257.
20. F. Barreca, C.R. Fichera, Energy Build. 62 (2013) 507.
21. V. Corinaldesi, J. Donnini, A. Nardinocchi, Lightweight plasters containing plastic waste for sustainable and energy-efficient building, Constr. Build. Mater. 94 (2015) 337.
22. J. Zhao, G. Huang, Y. Guo, R. Gupta, W. V. Liu, Constr. Build. Mater. 393 (2023) 132043.
23. https://www.mindat.org/min-1128.html
24. https://www.geologypage.com/2013/12/cordierite.html
25. N. Obradović, S. Filipović, N. Đorđević, D. Kosanović, V. Pavlović, D. Olćan, A. Đorđević, M. Kachlik, K. Maca, Sci. Sint 48:2 (2016) 157.
26. T. Boldizsár, H. Bali, I. Szenti, et al., J. Europ. Ceram. Soc. 43:13 (2023) 5596.
27. V. José da Silva, E. de Almeida, W. P. Gonçalves, et al., Ceram. Internat. 45:4 (2019) 4692.
28. V. Pereira, C. Rodrigues, F. Toniolo, Catalysis Communications 183 (2023) 106759.
29. Q. Yan, J. Ji, Y. Chen, G. Zhao, B. Jia, L. Xu, P. Cheng, App. Cataly. B: Envir. 343 (2024) 123530.
30. P. Kittl, G. Diaz, H. Alarcón, Cement Concr. Res. 22:5 (1992) 736.
31. P. Vincent Venkatesan, R. Suganya, S. Revathi, Materials Today: Proceedings 62 (2022) 4374.
32. D. Drdlik, K. Drdlikova, K. Maca, Sci. Sinter. 55 (2023) 289.
33. J. N. Sabouang, J.A. Mbey, Liboum, F. Thomas, D. Njopwouo, J. Asian Ceram. Soc. 2 (2014) 263.
34. United Nations Development Programme: https://www.undp.org › sustainable-development-goals
35. https://www.superbheater.com/materials-and-fitting/bobbin-heater-fitting-parts-and/high-quality-cordierite-ceramic.html.
36. SRPS EN 1015-2:2008 Methods of test for mortar for masonry - Part 2: Bulk sampling of mortars and preparation of test mortars
37. SRPS EN 1015-3:2008 Methods of test for mortar for masonry - Part 3: Determination of consistence of fresh mortar (by flow table)].
38. SRPS EN 1015-6:2008 Methods of test for mortar for masonry - Part 6: Determination of bulk density of fresh mortar.
39. SRPS EN 1015-10:2008/A1:2008 Methods of test for mortar for masonry - Part 10: Determination of dry bulk density of hardened mortar
40. SRPS EN 1015-18:2008 Methods of test for mortar for masonry - Part 18: Determination of water absorption coefficient due to capillary action of hardened mortar.,
41. SRPS EN 1015-18:2008 Methods of test for mortar for masonry - Part 18: Determination of water absorption coefficient due to capillary action of hardened mortar.
42. SRPS EN 1015-11:2019 Methods of test for mortar for masonry - Part 11: Determination of flexural and compressive strength of hardened mortar.
43. ASTM G32-16 Red Standard Test Method for Cavitation Erosion Using Vibratory Apparatus (Standard + Redline PDF Bundle) https://webstore.ansi.org/standards/astm/astmg3216red
44. A.W. Momber, Intern. J. Miner. Process. 74 (2004) 177.
45. M. Hauer, F. Gärtner, S. Krebs, S. et al. J Therm Spray Tech 30 (2021)1310.
46. A. Mohsen, I. Aiad, F.I. El-Hossiny, A.O. Habib, Egypt. J. Petrol. 29:2 (2020) 171.
47. A. Terzić, L. Pezo, Lj Andrić, M. Arsenović, Compos. B Eng. 79 (2015) 660.
48. A. Koehler, J. Neubauer, F. Goetz-Neunhoeffer, Cement 7 (2022) 100020.
49. V. Antonovič, J. Kerienė, R. Boris, M. Aleknevičius, Procedia Eng. 57 (2013) 99.
50. N. Bentaieb, D. Touil, A. Lachemet, R. Zirour, S. Belaadi, C. Frances, Chem. Eng. Trans. 24 (2011) 685.
51. F. Zunino, E. Boehm-Courjault, K. Scrivener, Mater. Struct. 53 (2020) 44.
52. C. Rodriguez-Navarro, E. Ruiz-Agudo, A. Luque, A. Rodriguez-Navarro, M. Ortega-Huertas, Am. Min. 94:4 (2009) 578.
53. M. Wesolowski, Thermal decomposition of talc: review, Thermochim. Acta 78 (1984) 395.

54. A. Wiewiora, S. Sanchez-Soto, M. Avilos, A. Justo, L. Perez-Maqueda, J. Perez-Rodriguez, P. Bylina, Appl. Clay Sci.12 (1997) 233.
55. S. K. Marikkannan, E. P. Ayyasamy, J. Mater. Res. Technol. 2 (2013) 269.
56. Z. Klika, M. Valášková, L. Bartoňová, P. Maierová, Minerals. 10 (2020) 1122.

Апстракт *У овом истраживању испитивана су својства термоизолационих малтера за екстеријер са различитим односом микронизираног кордиерита и талка. Циљ истраживања је био да се утврди да ли се рециклирани кордиерит може поново применити у дизајну малтера без значајног погоршања његових перформанси. За испитивање термичких реакција коришћена је диференцијална термичка анализа. Кавитациона ерозија, у секвенцама испитивања у распону од 30 до 120 минута, коришћена је за процену компактности структуре малтера. Физичко-механичка својства (укључујући чврстоћу на притисак и савијање и чврстоћу на притисак након печења на 1000°C) експерименталних малтера су испитана и упоређена са стандардним малтером. Морфологије пелета малтера након кавитације проучаване су помоћу скенирајућег електронског микроскопа. Утврђено је да кордиерит и талк као филер у количини до 20% побољшавају микроструктурно паковање и механичку чврстоћу због побољшане цементације и тиме доприносе отпорности на кавитациону ерозију. Веће количине талка изазивају значајнију деградацију структуре и губитак масе током кавитационих тестова. Смањење трошкова производње, потрошње енергије и емисије гасова стаклене баште главни су циљеви производње овог иновативног грађевинског композита базираног на отпадом ресурсу, јер поновна употреба отпадних материјала може помоћи у постизању низа циљева одрживог развоја.*

Кључне речи: *алтернативне сировине; синтеровање; диференцијална термичка анализа; микроструктура; испитивање на кавитацију.*